

Article

Stably Improving the Catalytic Activity of Oxygen Evolution Reactions via Two-Dimensional Graphene Oxide-Incorporated NiFe-Layered Double Hydroxides

Ling Chen ¹, Yue Lu ¹, Manman Duanmu ¹, Xin Zhao ¹, Shenglu Song ¹, Liyue Duan ¹, Zhipeng Ma ^{1,2}, Ailing Song ^{1,2,*}  and Guangjie Shao ^{1,2,*} 

- ¹ Hebei Key Laboratory of Applied Chemistry, College of Environmental and Chemical Engineering, Yanshan University, Qinhuangdao 066004, China; hhchen@ysu.edu.cn (L.C.); yueluysu@stumail.ysu.edu.cn (Y.L.); manman.duanmu@stumail.ysu.edu.cn (M.D.); zhaoxin729914@163.com (X.Z.); slsong@stumail.ysu.edu.cn (S.S.); liyue.duan@stumail.ysu.edu.cn (L.D.); mazp@ysu.edu.cn (Z.M.)
- ² State Key Laboratory of Metastable Materials Science and Technology, Yanshan University, Qinhuangdao 066004, China
- * Correspondence: ailing.song@ysu.edu.cn (A.S.); shaoguangjie@ysu.edu.cn (G.S.)

Abstract: NiFe-layered double hydroxides (NiFe-LDH) have been reported to possess exceptional oxygen evolution reaction (OER) activity. However, maintaining the stability of high activity over a long time remains a critical challenge that needs to be addressed for their practical application. Here, we report a custom-sized deep recombination of 2D graphene oxide with NiFe-LDH (NiFe-LDH/GO/NF) through a simple electrodeposition method that improves OER activity and achieves excellent stability. The excellent performance of the catalyst mainly comes from the three-phase interface and electron transport channel dredged by the three-dimensional structure constructed by the deep composite, which can not only significantly reduce its charge and electron transfer resistance, improving the material conductivity, but it also effectively increases the specific surface area, inhibits aggregation, and exposes rich active sites. In addition, GO with good conductivity not only supports NiFe-LDH well but also increases the heterogeneous interface, putting the NiFe-LDH/GO composites in close contact with Ni foam and increasing the electrocatalytic stability of the NiFe-LDH/GO/NF. The experimental results show that the overpotential of NiFe-LDH/20,000GO/NF is only 295 mV at a current density of 100 mA cm⁻²; the Tafel slope is 52 mV dec⁻¹, and the charge transfer resistance (*R*_{ct}) is only 0.601 Ω in 1 M KOH. This indicates that GO has excellent potential to assist in constructing geometric and electronic structures of NiFe-LDH in long-term applications.

Keywords: nickel-iron-layered double hydroxide; graphene oxide; oxygen evolution reaction



Citation: Chen, L.; Lu, Y.; Duanmu, M.; Zhao, X.; Song, S.; Duan, L.; Ma, Z.; Song, A.; Shao, G. Stably Improving the Catalytic Activity of Oxygen Evolution Reactions via Two-Dimensional Graphene Oxide-Incorporated NiFe-Layered Double Hydroxides. *Catalysts* **2024**, *14*, 278. <https://doi.org/10.3390/catal14040278>

Academic Editor: Lucjan Chmielarz

Received: 27 March 2024

Revised: 14 April 2024

Accepted: 17 April 2024

Published: 19 April 2024



Copyright: © 2024 by the authors. Licensee MDPI, Basel, Switzerland. This article is an open access article distributed under the terms and conditions of the Creative Commons Attribution (CC BY) license (<https://creativecommons.org/licenses/by/4.0/>).

1. Introduction

Hydrogen energy is a novel energy carrier that is considered a promising alternative to conventional fossil fuels. It is regarded as a sustainable and clean energy source with the potential to mitigate environmental issues. However, during the electrolysis of water for hydrogen evolution, the OER at the anode exhibits sluggish kinetics compared to the two-electron process of the electrocatalytic hydrogen evolution reaction at the cathode. This disparity between the anodic and cathodic processes significantly limits the overall efficiency of electrocatalytic water splitting [1–4]. Among them, the identification of active sites and the exploration of the relationship between material structure and performance play a crucial role in electrocatalytic water splitting [5]. For example, Pan et al. [6] designed Mg-substituted perovskite cobalt oxide salt (SCFM-01) with a co-customized cubic symmetric structure and fine electronic structure, achieving extremely high catalytic activity and considerable durability in OER (low overpotential of only 320 mV at 10 mA cm⁻²,

small Tafel slope of 65 mV dec^{-1}). Therefore, preparing efficient and stable electrochemical OER electrocatalysts to accelerate the reaction kinetics is an essential development in electrocatalysis [7–10]. In recent years, many works have reported on applying various modified materials in OER catalysts, mainly including precious-metal-based, non-precious, and non-metallic-based catalysts [11–14]. Precious metal catalysts (IrO_2 , RuO_2 , etc.) are still the choice for large-scale applications, but their high cost, scarcity, and poor stability in alkaline electrolytes greatly limit their practical application [15–18]. Researchers have been exploring many substitutes for precious metals in recent years. NiFe-LDH has emerged as a highly promising material due to its cost-effectiveness and impressive electrochemical properties [19–21]. This material boasts a unique structure with variable ions in layers, exchangeable anions between layers, and large reaction surfaces that can even compete with those of precious metals. As such, NiFe-LDH has garnered significant attention as a potential alternative to traditional precious metal catalysts [22–24]. However, NiFe-LDH has drawbacks such as poor conductivity, insufficient stability, and incompletely exposed active sites, which hinder the charge transfer between the catalyst surface and electrolyte interface, reducing catalytic activity [25–27]. Therefore, effective improvement strategies are still needed to optimize the properties and enhance the catalytic performance of NiFe-LDH [28–31].

Many efforts have been reported to integrate various active components to optimize the catalytic performance of NiFe-LDH electrocatalysts in OER [32–35]. An effective strategy is to promote electrolyte diffusion and optimize the desorption of gas products by increasing the electrochemically active surface area (ECSA) of the material [36–39]. For example, Feng et al. [40] used a simple hydrothermal method to integrate NiFe-LDH into NiCo_2S_4 to form a heterostructure of a novel cactus-like structure with highly exposed ECSA. The prepared $\text{NiCo}_2\text{S}_4/\text{NiFe-LDH}$ hollow spheres greatly enhance the OER activity, with an overpotential of only 287 mV at 10 mA cm^{-2} , even lower than commercial IrO_2 (400 mV). In addition to increasing the ECSA in the material, conductivity can also be improved by composites with multiple materials, reducing their charge and electron transfer resistance to accelerate the kinetics of the OER [41]. For example, Xu et al. [42] prepared a series of RP/SP (single perovskites/Ruddlesden–Popper perovskites) perovskite composites with the same phase structure and composition but different phase concentrations through a simple cation deficiency strategy. The strong coupling between RP and SP phases enhanced ion transport and improved material conductivity. For example, Du et al. [43] used a one-step coprecipitation method to disperse CeO_{2-x} particles on the NiFe-LDH, forming a $\text{CeO}_{2-x}/\text{NiFe-LDH}$ heterostructure. Through the electronic interaction between Ni, O, and Ce, the high potential barrier of OER is effectively reduced. At a current density of 10 mA cm^{-2} , $150 \text{ CeO}_{2-x}/\text{NiFe-LDH}$ exhibits the lowest overpotential of 216 mV. Shen et al. [37] used an efficient solid-phase exfoliation strategy to exfoliate NiFe-LDH and GO into monolayer nanosheets and then combined them to obtain a composite material NFCG nanohybrid and explore its OER activity in alkaline solutions. The experimental results indicated that the unique three-dimensional class array heterostructure of NFCG nanohybrids can expose many active sites, and the strong coupling between NiFe-LDH-NS and RGO-NS leads to rapid electron transfer, which positively improves the catalytic performance of the NFCG catalysts. The optimized NFCG-3 exhibits excellent OER catalytic performance with an overpotential of 273 mV at a current density of 30 mA cm^{-2} and a Tafel slope of 49 mV dec^{-1} . Therefore, it has been demonstrated that effective assembly recombination can be employed as a viable strategy for designing and enhancing the electrocatalytic performance of NiFe-LDH active materials in OER [37,44–46].

In this work, to optimize the catalytic performance of NiFe-LDH electrocatalysts in OER, a two-dimensional GO was tightly composited with NiFe-LDH in rich channels on nickel foam (NiFe-LDH/GO/NF) by a one-step electrodeposition method. The main focus was to investigate the effects of different mesh sizes of GO (10,000 mesh, 15,000 mesh, 20,000 mesh) on the structural construction and electrochemical performance of composite materials. The resulting composite material has shown promising results in improving

the catalytic activity of NiFe-LDH. Experiments have shown that the prepared NiFe-LDH/GO/NF nanostructures have a high specific surface area, significantly promoting the exposure of surface active sites. The composite structure composed of GO and NiFe-LDH not only effectively increases the specific surface area to expose rich active sites but also enhances the conductivity of NiFe-LDH and improves its electron and ion transport capabilities. Electrochemical tests have shown that the optimized NiFe-LDH/20,000GO/NF exhibits excellent OER performance, with an overpotential of only 295 mV at a current density of 100 mA cm^{-2} , a Tafel slope of 52 mV dec^{-1} , and an excellent stable operation up to 200 h. The suitable combination size customized three-dimensional channel structure is anticipated to enhance the catalytic activity of the composite by facilitating mass and electron transfer of the reactants at the nanoscale, resulting in a remarkable improvement in the overall catalytic performance.

2. Results and Discussion

2.1. Material Synthesis and Characterization

Figure 1 displays schematic illustrations of NiFe-LDH/GO/NF and NiFe-LDH/NF composites, which were synthesized using a simple one-step electrodeposition method. During the process of electrodeposition, Ni foam is immersed in an electrolyte. When GO and NiFe-LDH are deposited together, the color of the Ni foam changes from silver gray to dark yellow. When only NiFe-LDH is deposited, the structure becomes challenging to present an excellent three-dimensional morphology due to the lack of support. In contrast, when GO is added to the deposition, the composite deposition of GO and NiFe-LDH provides structural support to NiFe-LDH, resulting in a good three-dimensional multi-channel structure. When GO with good conductivity matches the size of NiFe-LDH, this channel enhances the exposure of the three-phase interface and the transport of electrons in terms of geometry and electronic structure, respectively.

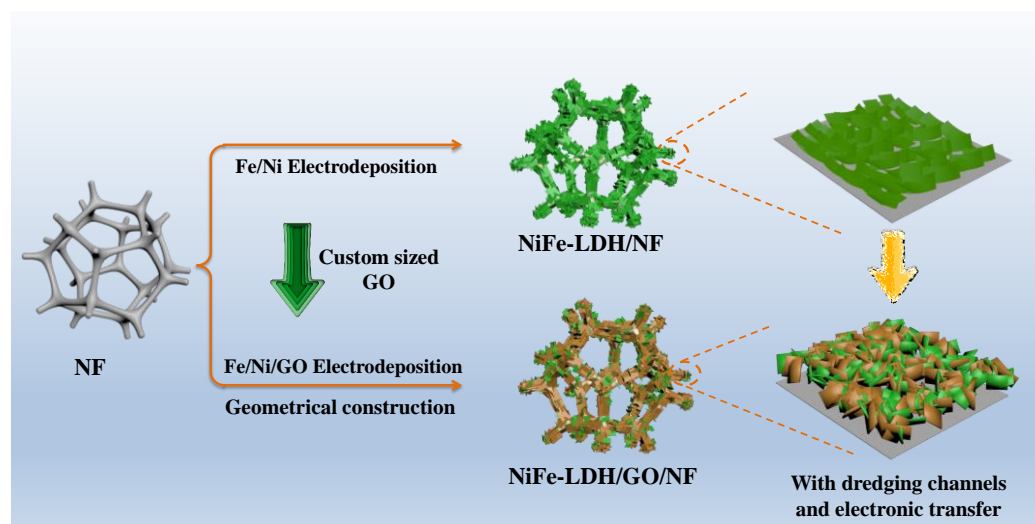


Figure 1. Schematic illustration of the synthesis of NiFe-LDH/GO/NF and NiFe-LDH/NF composite materials.

The morphology of catalysts obtained by electrodeposition was characterized by field emission scanning electron microscopy (FESEM) and transmission electron microscopy (TEM). Figure 2a,b show the SEM images of the NiFe-LDH/NF and NiFe-LDH/20,000GO/NF composites, respectively. Ni foam has a three-dimensional porous structure with many pores and a well-preserved skeleton structure. As shown in Figure 2a, it is observed that NiFe-LDH grows in situ on the Ni foam skeleton with a relatively small size, ensuring a firm interface connection without the role of a binder, thus promoting the flow of electrons from the catalyst array to the electrode during anodic polarization. It can also be seen that

NiFe-LDH materials are interconnected and stacked on the Ni foam substrate in the form of nanosheet arrays. Figure 2b shows the SEM image of the material after introducing 20,000 mesh GO. Compared to NiFe-LDH/NF, the material grown on the Ni foam skeleton in NiFe-LDH/GO/NF was found to have a denser distribution after introducing GO. It can be seen that the morphology after adding GO changed. GO and NiFe-LDH with opposite charges form stacked nanostructures under electrostatic attraction and vertically cross into uniform porous channel structures distributed on the surface of Ni foam. The open porous channel structure is conducive to the desorption of bubbles generated during electrode reaction, promoting the catalyst to make contact with the solution during the electrode reaction and preventing the mass rate from being too slow due to the stacking of bubbles. Figures 2c,d and S1 show the TEM image of the NiFe-LDH/NF, NiFe-LDH/20,000GO/NF, NiFe-LDH/10,000GO/NF, and NiFe-LDH/15,000GO/NF nanocomposites, providing more precise evidence of the layered structure of GO and LDH nanosheets stacked together, confirming that the NiFe-LDH/20,000GO/NF composite is a nanoscale layered structure. As can be seen from Figure 2a,c, the NiFe-LDH laid on the Ni foam is slightly convex, and the connection between the catalyst and the support is not tight, making it easy to fall off and have poor stability, resulting in catalyst inactivation. As can be seen from Figure 2b,d, the heterogeneous interface with the substrate is increased after forming a composite with GO. In addition, the robust three-dimensional network constructed by NiFe-LDH/GO and its tighter connection to the Ni foam enhance the stability of the NiFe-LDH/GO/NF. As shown in Figure 2e–j, EDS elemental spectrum analysis shows that Ni, Fe, O, and C elements are uniformly distributed on the nanosheets. The results obtained herein provide unequivocal evidence of the strong and synergistic combination of GO and NiFe-LDH, as well as the establishment of a three-dimensional channel structure.

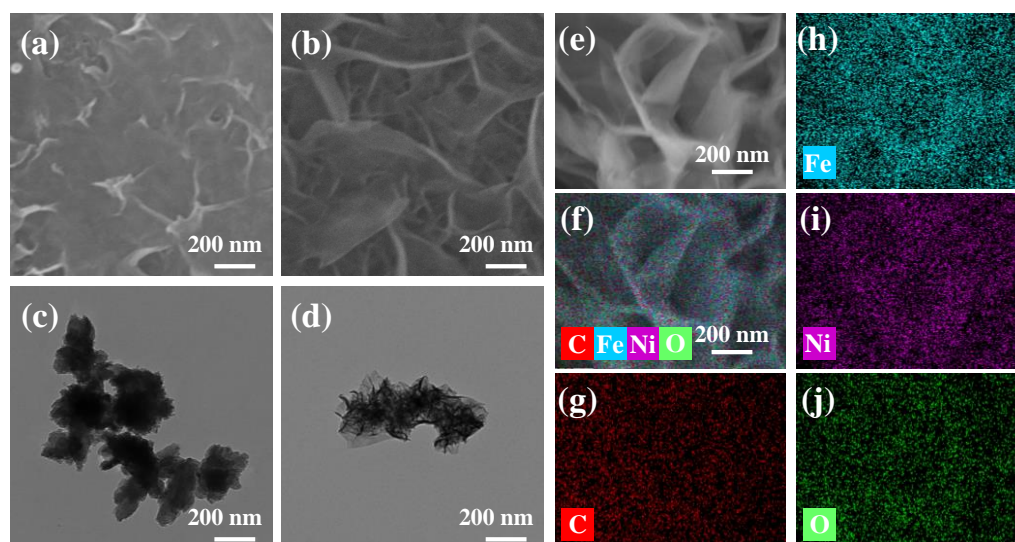


Figure 2. The SEM images of (a) NiFe-LDH/NF and (b) NiFe-LDH/20,000GO/NF. The TEM images of (c) NiFe-LDH/NF and (d) NiFe-LDH/20,000GO/NF. (e–j) The SEM images and the corresponding elemental mapping images of the NiFe-LDH/20,000GO/NF.

X-ray diffraction (XRD) is one of the most important techniques for evaluating the crystal structure of NiFe-LDH/GO/NF composites. As shown in Figure 3a, the peak located at 10.5° is a characteristic peak that matches the (001) surface of GO. The peaks located at 10.1° , 21.4° , 34.08° , and 60.4° belong to the (003), (006), (012), and (110) planes of NiFe-LDH (JCPDS No. 40-0215). In addition, as the GO mesh size increases, the diffraction peak of the sample becomes significantly stronger. The calculated crystallinity of NiFe-LDH/20,000GO/NF was 0.7867, higher than that of NiFe-LDH/10,000GO/NF (0.6324) and NiFe-LDH/15,000GO/NF (0.6858). The results also display that the introduction of GO causes the peaks of graphene of NiFe-LDH/GO to shift to the left, leading to larger

interplanar spacing. In general, the crystallinity of the catalyst is proportional to the intermolecular force. The above results indicate that the bonding force and structural stability of NiFe-LDH in NiFe-LDH/20,000GO/NF is strengthened. In addition, as shown in Figure 3b, GO, NiFe-LDH/10,000GO/NF, NiFe-LDH/15,000GO/NF, and NiFe-LDH/20,000GO/NF all show similar double Raman absorption peaks corresponding to the D band and G band of graphene at 1351 cm^{-1} and 1585 cm^{-1} , indicating the presence of GO in nanohybrids. The characteristic peaks at 451 cm^{-1} and 528 cm^{-1} can be attributed to the Ni–O and Fe–O bonds indexed to $\text{Ni}(\text{OH})_2$ and FeOOH , indicating the presence of NiFe-LDH. The R value (I_D/I_G) of NiFe-LDH/20,000GO/NF calculated in the peak area is 2.266, which is higher than the R values of NiFe-LDH/10,000GO/NF (1.797) and NiFe-LDH/15,000GO/NF (1.938), indicating that the GO in the sample has higher disorder and larger defects, which is in accordance with the results of XRD.

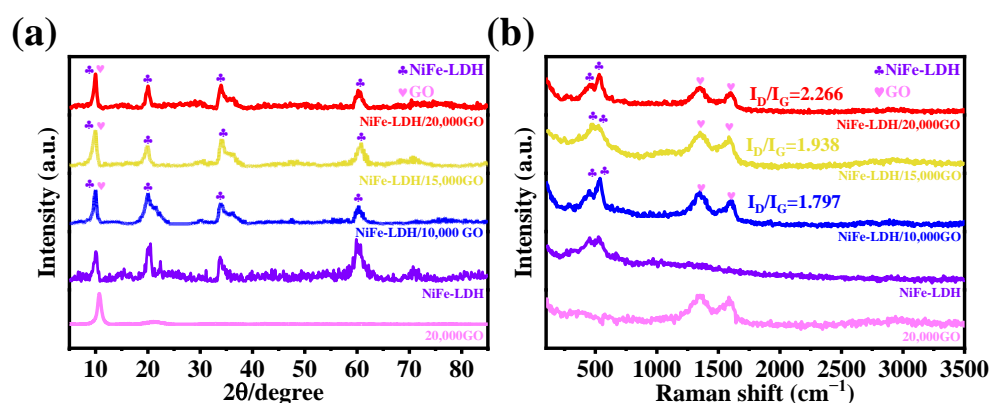


Figure 3. (a) XRD patterns; (b) Raman spectra of 20,000GO, NiFe-LDH/NF, NiFe-LDH/10,000GO/NF, NiFe-LDH/15,000GO/NF, and NiFe-LDH/20,000GO/NF.

The surface bonding state of the catalyst was further characterized using X-ray photoelectron spectroscopy (XPS). In Figure 4a, the NiFe-LDH/20,000GO/NF is mainly composed of four elements: Ni, Fe, O, and C. Figure 4b shows the high-resolution Ni $2p$ spectrum which has two characteristic peaks at 855.28 and 872.86 eV, corresponding to Ni $2p_{3/2}$ and Ni $2p_{1/2}$. Figure 4c shows the high-resolution Fe $2p$ spectra at 725.49, 713.05, 720.12, and 707.32 eV, corresponding to Fe^{3+} ($2p_{1/2}$ and $2p_{2/3}$) and Fe^{3+} ($2p_{1/2}$ and $2p_{2/3}$). The high-resolution C $1s$ spectra of the hybrids in Figure 4d have four peaks; the binding energies at 283.86, 287.73, 288.65, and 284.62 eV correspond to the C–C/C=O, –C–OH, C–O–C, and C=O, respectively. Compared with the peak of NiFe-LDH/NF, after forming a composite with GO, the corresponding peak of Ni $2p$ shifts to a lower energy level by 0.75 eV, while the corresponding peak of Fe $2p$ shifts to a lower energy level by 0.49 eV. XPS shows that after GO and NiFe-LDH are compounded, the electronic structure is adjusted, thus improving the catalytic activity and stability of the material.

2.2. Electrochemical Activity towards OER

Electrochemical tests were conducted in a 1 M KOH solution ($\text{pH} \approx 14$) to evaluate the electrocatalytic OER activity of different samples. Based on a three-electrode system, carbon rods were used as counter electrodes, and Hg/HgO was used as a reference electrode. Bare NF, RuO_2 , 20,000GO/NF, NiFe-LDH/NF, and NiFe-LDH/20,000GO/NF electrodes were characterized and compared. Linear sweep voltammetry (LSV) was used for testing, and all polarization curves were compensated by iR . As shown in Figure 5a,b, compared to bare NF (625 mV), RuO_2 (310 mV), 20,000GO/NF (402 mV), and NiFe-LDH/NF (350 mV), the NiFe-LDH/20,000GO/NF shows the lowest overpotential of 295 mV (145 mV for 10 mA cm^{-2}) at the current density of 100 mA cm^{-2} . This is better than the NiFe-LDH/GO prepared using other methods in previous research by others [37]. The Tafel slope can reflect the dynamic process of the electrode during oxygen evolution. Figure 5c shows the Tafel slope obtained by fitting the strong polarization region of the LSV curve. The smaller the Tafel

slope, the smaller the change in overpotential with the increase in current density, and the better the electrocatalytic performance. The Tafel slope of NiFe-LDH/20,000GO/NF is only 52 mV dec^{-1} , which is lower than that of bare NF (127 mV dec^{-1}), RuO_2 (59 mV dec^{-1}), 20,000GO/NF (65 mV dec^{-1}), and NiFe-LDH/NF (55 mV dec^{-1}). The lower Tafel slope of NiFe-LDH/20,000GO/NF indicates that the material has fast kinetics for oxygen evolution. Compared to similar work in the same period, it is superior to other samples [47–51].

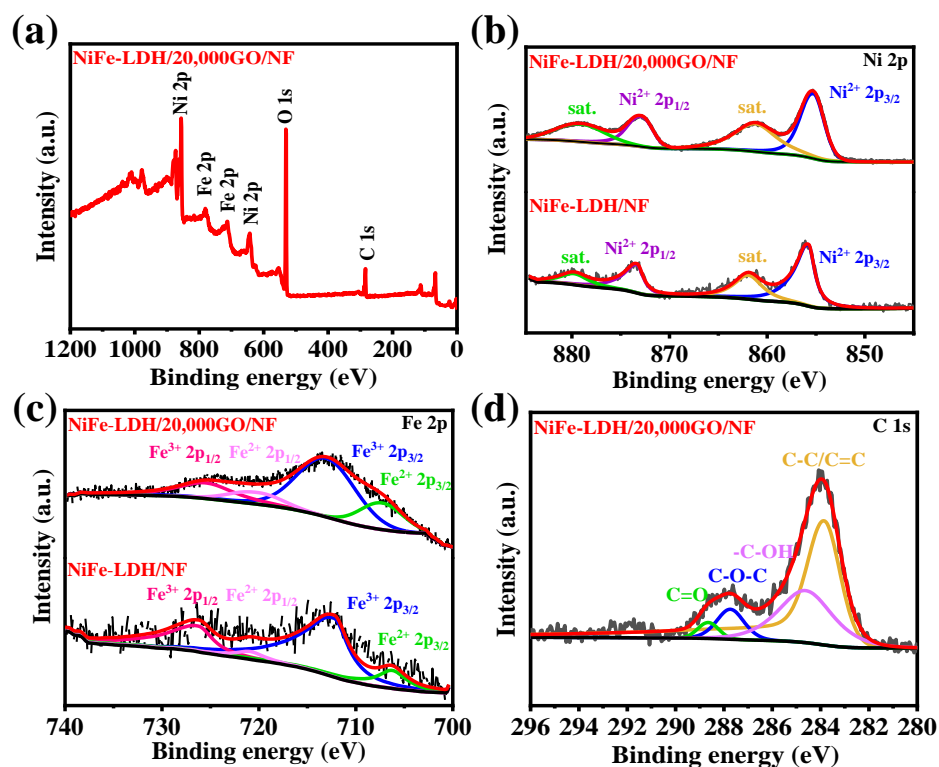


Figure 4. (a) XPS survey spectra of NiFe-LDH/20,000GO/NF and NiFe-LDH/NF; high-resolution XPS spectra of (b) Ni 2p, (c) Fe 2p, and (d) C 1s.

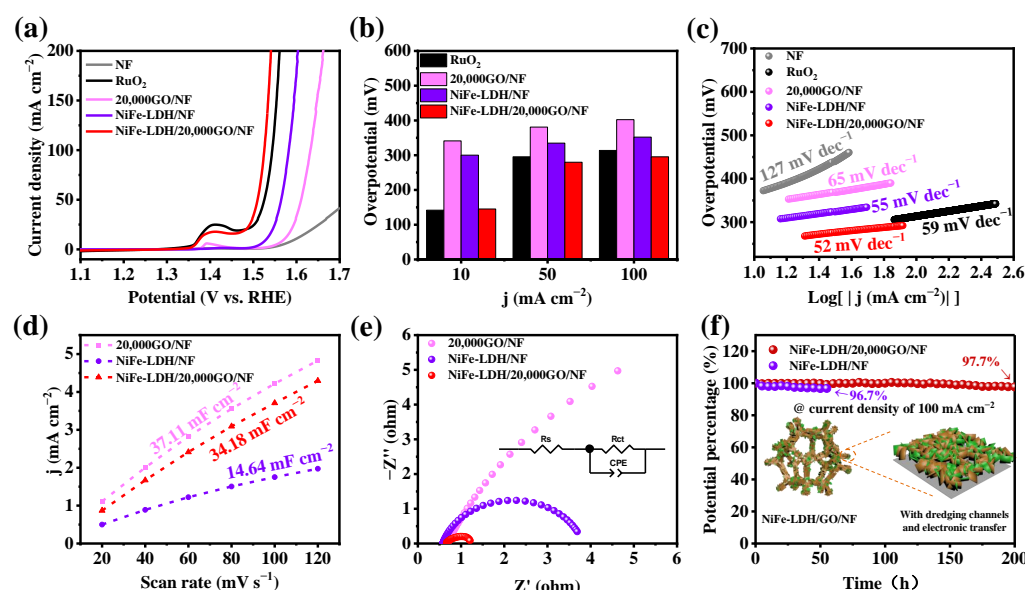


Figure 5. (a) iR-corrected LSV polarization curves, (b) overpotential at 10, 50, and 100 mA cm^{-2} , (c) Tafel slope, (d) ECSA estimated by C_{dl} values, and (e) EIS plot of different catalysts. (f) The chronopotentiometry plot of NiFe-LDH/20,000GO/NF and NiFe-LDH/NF at 100 mA cm^{-2} .

The ECSA of catalysts plays a crucial role in the reaction, and the double-layer capacitance value (C_{dl}) is directly proportional to the ECSA value. The C_{dl} of different samples can be compared by comparing slope values. The C_{dl} usually infers the ECSA value of catalysts. Figure S2 shows the cyclic voltammetry (CV) curves of 20,000GO/NF, NiFe-LDH/NF, and NiFe-LDH/20,000GO/NF. In the voltage range of 0~0.1 V vs. Hg/HgO, the polarization current density contrast of the cathode and anode corresponding to the scanning speed and the middle voltage under different scanning speeds ($\Delta J = j_a - j_c$) is plotted as a linear graph. As shown in Figure 5d, the C_{dl} value calculated from the CV curves of NiFe-LDH/20,000GO/NF is 34.18 mF cm^{-2} , higher than that of NiFe-LDH/NF (14.64 mF cm^{-2}) and slightly lower than 20,000GO/NF. Based on the proportional relationship between ECSA and C_{dl} , the results indicate that the small-size GO prepared from high-mesh graphite has a high ECSA value, meaning a larger surface area exposure. Furthermore, the combination of NiFe-LDH and GO effectively supports the structure of NiFe-LDH obtained by electrodeposition, resulting in full exposure to the active sites.

The charge transfer rate of the electrode was further analyzed using electrochemical impedance spectroscopy (EIS). As shown in Figure 5e, the EIS curves of different samples were fitted using the equivalent circuit shown in the illustration. R_{ct} is the charge transfer resistance at the interface between the electrode and electrolyte. It can be seen that the R_{ct} of NiFe-LDH/20,000GO/NF is the smallest, 0.601Ω , which is better than that of 20,000GO/NF (1.37Ω) and NiFe-LDH/NF (3.244Ω). In addition, Figure 5f shows the stability tests of NiFe-LDH/NF and NiFe-LDH/20,000GO/NF under chronopotentiometry at a current density of 100 mA cm^{-2} . A significant increase in the overpotential of NiFe-LDH/NF was observed only after 50 h. NiFe-LDH/20,000GO/NF can still maintain a 97.7% overpotential retention rate after 200 h of testing, and there is no significant change in the bonding state of the material surface after testing. To verify the contribution of GO to electron transport during the continuous catalytic reaction, we performed XPS characterization on the tested samples. As shown in Figure 6a–d, the spectra of C 1s and Fe 2p are shifted to the direction of high binding energy for $\sim 0.17 \text{ eV}$ and $\sim 0.11 \text{ eV}$, which means that both lose electrons during the reaction, while the spectrum of Ni 2p is shifted to the direction of low binding energy at $\sim 0.52 \text{ eV}$, which means that Ni gains electrons during the reaction. This further demonstrates the electron donor role of GO during the reaction.

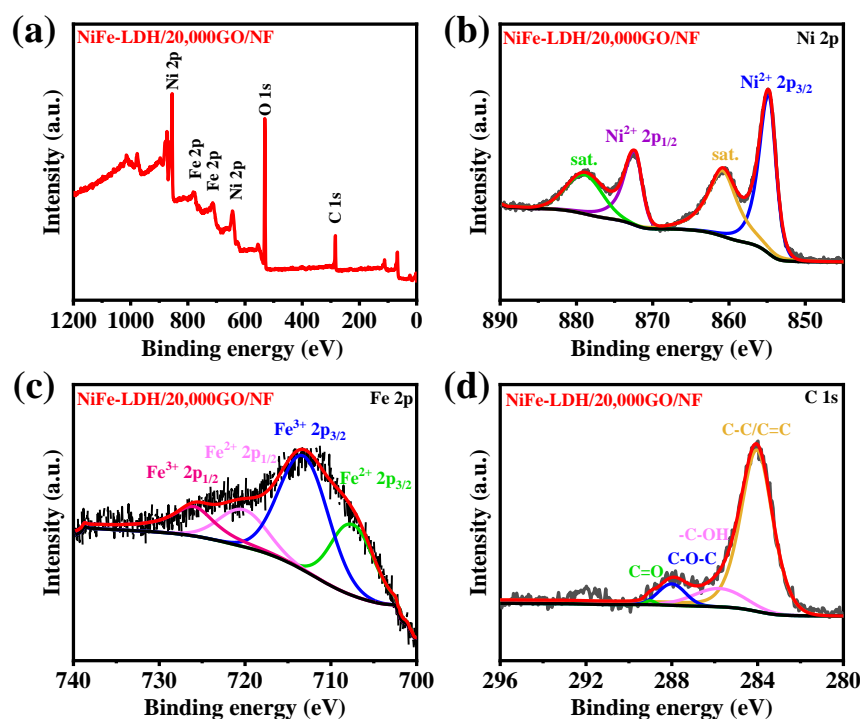


Figure 6. (a–d) XPS spectra of NiFe-LDH/20,000GO/NF after stability test for 200 h.

In this experiment, GO prepared by graphite with different mesh numbers can also affect the catalytic performance of the composite material. The three composite materials, NiFe-LDH/10,000GO/NF, NiFe-LDH/15,000GO/NF, and NiFe-LDH/20,000GO/NF, were prepared for comparison. Figure 7a shows the LSV curves of different samples. At a current density of 100 mA cm^{-2} , NiFe-LDH/20,000GO/NF has the lowest overpotential of 295 mV, which is lower than NiFe-LDH/10,000GO/NF (330 mV) and NiFe-LDH/15,000GO/NF (210 mV). In addition, Figure 7b shows that the Tafel slope of NiFe-LDH/20,000GO/NF is also the lowest, lower than NiFe-LDH/10,000GO/NF (61 mV dec^{-1}) and NiFe-LDH/15,000GO/NF (54 mV dec^{-1}). These results indicate that the size of GO can affect the catalytic kinetics of the composite material. Then, the C_{dl} values of different samples were calculated for comparison (Figure S3). As shown in Figure 7c, it can be seen that the C_{dl} value of NiFe-LDH/10,000GO/NF is the highest at 56.11 mF cm^{-2} . The C_{dl} values of NiFe-LDH/15,000GO/NF and NiFe-LDH/20,000GO/NF are 26.45 mF cm^{-2} and 34.18 mF cm^{-2} , respectively. The reason for this phenomenon is that GO with a size of $\sim 500 \text{ nm}$ (Figure S4a) in 10,000GO is relatively larger in two dimensions, which makes it difficult to fully recombine with the NiFe-LDH. Meanwhile, the high ECSA obtained from NiFe-LDH/10,000GO testing is due to the exposure of GO, which is not accompanied by an increase in active surface area. When the size of GO is reduced to $\sim 300 \text{ nm}$ (Figure S4b) in 15,000GO, the C_{dl} decreases, but it is still not sufficient to support NiFe-LDH because of incomplete recombination. However, at a size of $\sim 200 \text{ nm}$ (Figure S4c), 20,000GO can be fully recombined with NiFe-LDH, resulting in three-dimensional channel structures, thereby increasing the active sites and enhancing the charge transfer ability. Figure 7d shows the EIS curves of different samples. The R_{ct} of NiFe-LDH/20,000GO/NF is the smallest at 0.601Ω , which means that the charge transfer rate of NiFe-LDH/20,000GO/NF is faster than that of NiFe-LDH/10,000GO/NF (1.786Ω) and NiFe-LDH/15,000GO/NF (1.248Ω).

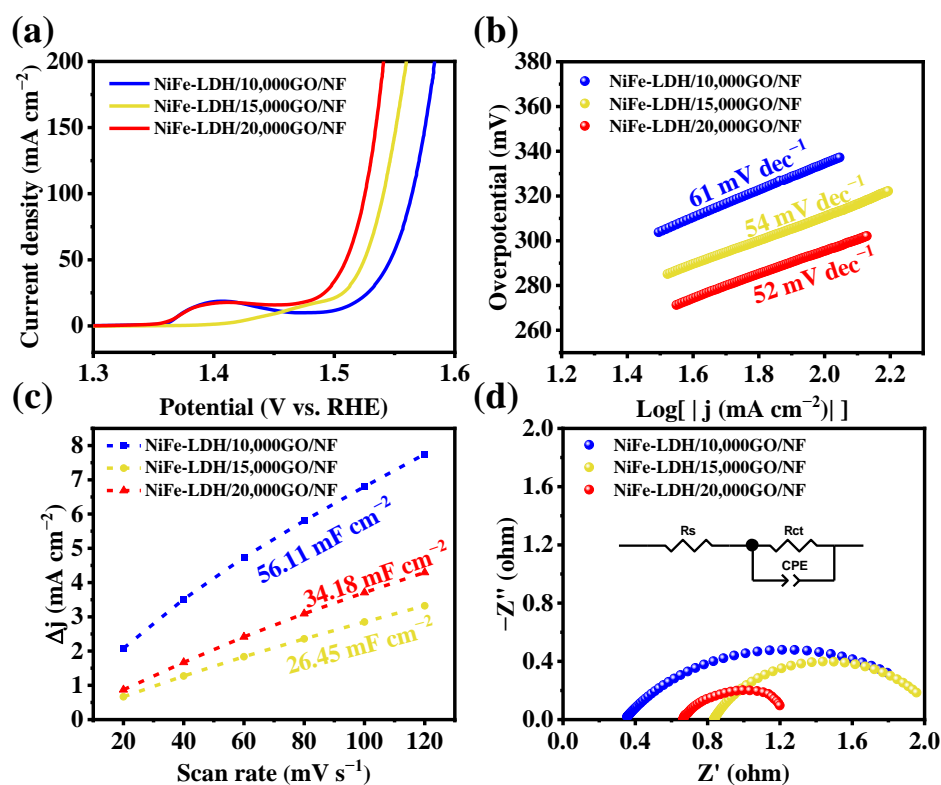


Figure 7. (a) iR-corrected LSV polarization curves, (b) Tafel slope, (c) ECSA estimated by C_{dl} values, and (d) EIS plot of different catalysts.

These results indicate that the NiFe-LDH/20,000GO/NF exhibits excellent catalytic activity and stability. The improvement in OER performance of NiFe-LDH/20,000GO/NF is due to two reasons: (1) The GO composite has a positive effect on preventing the re-accumulation of NiFe-LDH/NF, inhibiting aggregation and exposing more active sites of NiFe-LDH. (2) The introduction of GO with opposite charges forms channel nanostructures, facilitating the electrolyte and gas diffusion and enhancing electron transfer and the conductivity of NiFe-LDH. In summary, the reduction in overpotential and the improvement in durability are critically dependent on the exposure of active sites and charge transfer processes. Of notable significance is the optimal matching of GO and NiFe-LDH on Ni foam, which creates a remarkable synergistic effect, thus exploiting the full potential of NiFe-LDH and the electron supply effect of GO. This culminates in an effective enhancement of the density of active sites exposed by the composite material and significantly boosts the charge transfer ability of the reaction process.

3. Materials and Methods

3.1. Materials and Chemicals

All chemical substances are analytical reagents and used without further purification. Ni foam (battery grade, Lizhiyuan Technology Co., Ltd., Shenzhen, China), acetone (C_3H_6O , AR, Tianjin Jindongtianzheng Precision Chemical Reagent Factory, Tianjin, China), anhydrous ethanol (C_2H_6O , AR, Tianjin Kermel Chemical Reagent Co., Ltd., Tianjin, China), nickel nitrate hexahydrate ($Ni(NO_3)_2 \cdot 6H_2O$, AR, Tianjin Kaitong Chemical Reagent Co., Ltd., Tianjin, China), ferrous sulfate heptahydrate ($FeSO_4 \cdot 7H_2O$, Shanghai Macklin Biochemical Technology Co., Ltd., Tianjin, China), graphene oxide ($C_6O_{11}(OH)_2$, self-made), potassium hydroxide (KOH, AR, Tianjin Kermel Chemical Reagent Co., Ltd., Tianjin, China), a platinum electrode (Pt), a mercury oxide electrode (Hg/HgO), and deionized water were used in all experiments.

3.2. Preparation of NiFe-LDH/GO/NF

Pretreatment of nickel foam: The Ni foam (2 cm × 4 cm) was sonicated in acetone, ethanol, and deionized water for 30 min, respectively, to remove the surface oxide layer. Before the electrodeposition step, the pretreated nickel foam was ultrasonically washed with acetone, ethanol, and deionized water for 5 min to remove surface impurities.

Electrolyte preparation: First, graphite of 10,000 mesh, 15,000 mesh, and 20,000 mesh was taken to prepare GO. Weigh different sizes of GO and mix each with deionized water into a 40 mL solution. Stir and sonicate the solution. The specific processing method is to stir for 10 min, then sonicate for 30 min, and then stir again for 10 min, repeating multiple times until the GO is evenly dispersed. The ultrasonic process controls the water temperature between 10 and 15 °C. Add 3.489 g of $Ni(NO_3)_2 \cdot 6H_2O$ and 3.336 g of $FeSO_4 \cdot 7H_2O$ to GO dispersions with different mesh sizes, then add deionized water to prepare the solution to 80 mL. Stir magnetically to obtain three portions of an 80 mL electrolyte. The final concentration of $Ni(NO_3)_2$ and $FeSO_4$ in the electrolyte is 0.15 M.

Electrodeposition step: To thoroughly combine GO with metal cations, the electrolyte was subjected to magnetic stirring for 5 h before electrodeposition as a pretreatment process. The electrodeposition process was carried out using the Xinwei charge–discharge tester: the reference electrode was a saturated calomel electrode (SCE), and the double anode deposition method was used: Ni foam (2 cm × 4 cm) was used as the counter electrode, the double working electrode was two Pt sheet electrodes, and the reference electrode was a saturated calomel electrode (SCE). The working parameters were selected as a constant voltage charging of 1V, a deposition time of 60 s, and continuous magnetic stirring of the electrolyte during the deposition process to ensure a uniform solution. The deposited samples were washed with distilled water and dried overnight at 60 °C. The final experimental samples were recorded as NiFe-LDH/10,000GO/NF, NiFe-LDH/15,000GO/NF, and NiFe-LDH/20,000GO/NF.

3.3. Material Characterization

Field emission scanning electron microscopy (FESEM, Carl Zeiss Super55 (Carl Zeiss NTS GmbH, Oberkochen, Germany) operated at 15 kV) was carried out to observe the morphology of the samples. Transmission electron microscopy (TEM) images were obtained using a Hitachi HT7700 electron microscope (HITACHI Transmission Electron Microscope, Tokyo, Japan) at 120 kV. The phase composition and crystal structure were characterized by X-ray diffraction (XRD, RigakuSmart Lab, X-ray Diffractometer, Tokyo, Japan) at a scanning rate of 5° min^{-1} . Raman spectroscopy was utilized with the Horiba JY Xplora Plus instrument to perform microstructure analysis of the samples. X-ray photoelectron spectroscopy (XPS, ThermoFisher Nexsa, Fanrui Yunzhi Technology (Zhengzhou) Co., Ltd., Zhengzhou, China) was used to analyze the chemical composition and charge transfer of the samples.

3.4. Oxygen Evolution Reaction Test

Electrochemical tests showed that the composite material exhibits excellent OER performance, with an overpotential of only 295 mV and a Tafel slope of 52 mV dec^{-1} at a current density of 100 mA cm^{-2} . Electrochemical testing was conducted using the CHI660E workstation (CHI Instruments, Shanghai, China) to evaluate the OER electrocatalytic performance at room temperature. The traditional three-electrode system was used in the test: a saturated Hg/HgO electrode as the reference electrode, the composite material grown in situ on Ni foam ($1 \text{ cm} \times 1 \text{ cm}$) as the working electrode, and a Pt sheet electrode as the counter electrode. All electrochemical tests used 1 M KOH as the electrolyte (alkaline medium pH = 14). Linear sweep voltammetry (LSV) and CV curves were tested at a scanning rate of 5 mV s^{-1} from 0 to 1.0 V. The polarization curves were all corrected through manual iR compensation, with $E_{\text{cal}} = E_{\text{mea}} - i \cdot R_s \cdot A$ (E_{cal} is the potential after iR compensation, E_{mea} is the actual test potential, i is the actual test current, R_s is the solution internal resistance obtained through Nyquist curve fitting, and A is the coefficient considering compensation, all of which are taken as 100% in this paper). We collected electrochemical impedance spectroscopy (EIS) data at an AC voltage of 5 mV from 100 kHz to 0.01 Hz. The electrochemical surface area (ECSA) was obtained by measuring different scan rates based on CV plots in the scanning rate range of 20, 60, 100, 140, and 180 mV s^{-1} (v) lower Δj ($\Delta j = C_{\text{dl}} \cdot v$). We fitted the slope to obtain the double-layer capacitance (C_{dl}) to evaluate the ECSA value. ECSA can be calculated using the equation $\text{ECSA} = C_{\text{dl}}/C_s$, where C_s is the specific capacitance of the sample in an alkaline solution, typically 0.040 mF cm^{-2} . To evaluate the stability of the prepared catalysts, the v - t curve was obtained using chronopotentiometry at a current density of 10 mA cm^{-2} . This article uniformly uses the standard hydrogen potential as the standard potential.

$$E \text{ (vs. RHE)} = E \text{ (vs. Hg/HgO)} + E_{\text{Hg/HgO}} + 0.592\text{pH} \quad (1)$$

Overpotential (η) calculation:

$$\eta = E(\text{vs. RHE}) - 1.23\text{V} \quad (2)$$

4. Conclusions

In summary, a one-step electrodeposition method was used to deposit negatively charged GO and positively charged NiFe-LDH simultaneously. Through the regulation of GO size, the two similar sizes in the deposition process were closely combined and deposited on the three-dimensional Ni foam substrate in the form of multi-channel construction. The three-phase interface required for OER was effectively constructed, the electrochemically active surface area was increased, the charge and electron transfer resistance were reduced, and the conductivity and stability of the material were improved. The composite catalyst has the highest catalytic activity when the mesh number of graphite is 20,000. At a current density of 100 mA cm^{-2} , the overpotential of NiFe-LDH/20,000GO/NF is only 295 mV, and the slope of Tafel is 52 mV dec^{-1} , which is better than the performance

of most NiFe-based powder catalysts. In addition, the catalyst also exhibited excellent stability in the durability test for 200 h. This provides a new direction for finely modifying NiFe-based materials to obtain better OER catalytic performance and provides insights into the interaction between GO and NiFe-LDH.

Supplementary Materials: The following supporting information can be downloaded at <https://www.mdpi.com/article/10.3390/catal14040278/s1>: Figure S1: SEM images of (a) NiFe-LDH/10,000GO/NF and (b) NiFe-LDH/15,000GO/NF; Figure S2: CV curves of (a) 20,000GO/NF, (b) NiFe-LDH/NF, and (c) NiFe-LDH/20,000GO/NF; Figure S3: CV curves of (a) NiFe-LDH/10,000GO/NF and (b) NiFe-LDH/15,000GO/NF.

Author Contributions: Conceptualization, A.S. and G.S.; methodology, L.C.; validation, Y.L. and M.D.; formal analysis, L.C.; investigation, Y.L.; data curation, X.Z., S.S., and L.D.; writing—original draft preparation, L.C. and Y.L.; writing—review and editing, A.S.; resources, Z.M. and G.S.; supervision, A.S. and G.S. All authors have read and agreed to the published version of the manuscript.

Funding: This work was financially supported by the Hebei Province Natural Science Foundation Innovation Group Project (E2023203209), the National Natural Science Foundation of China (52174281), the Subsidy for Hebei Key Laboratory of Applied Chemistry after Operation Performance (22567616H), funding from the Hebei Provincial Department of Human Resources and Social Security (C20230328), and Yanshan University (8190410).

Data Availability Statement: Research data are not shared.

Conflicts of Interest: The authors declare no conflicts of interest.

References

1. Munonde, T.S.; Zheng, H.T.; Nomngongo, P.N. Ultrasonic exfoliation of NiFe LDH/CB nanosheets for enhanced oxygen evolution catalysis. *Ultrason. Sonochem.* **2019**, *59*, 104716. [CrossRef]
2. Bai, L.; Song, A.; Lei, X.; Zhang, T.; Song, S.; Tian, H.; Liu, H.; Qin, X.; Wang, G.; Shao, G. Hierarchical construction of hollow NiCo₂S₄ nanotube@NiCo₂S₄ nanosheet arrays on Ni foam as an efficient and durable electrocatalyst for hydrogen evolution reaction. *Int. J. Hydrogen Energy* **2022**, *47*, 38524. [CrossRef]
3. Song, A.; Song, S.; Duanmu, M.; Tian, H.; Liu, H.; Qin, X.; Shao, G.; Wang, G. Recent Progress of Non-Noble Metallic Heterostructures for the Electrocatalytic Hydrogen Evolution. *Small Sci.* **2023**, *3*, 2300036. [CrossRef]
4. Song, S.; Song, A.; Bai, L.; Duanmu, M.; Wang, L.; Dong, H.; Qin, X.; Shao, G. Hierarchical Design of Homologous NiCoP/NF from Layered Double Hydroxides as a Long-Term Stable Electrocatalyst for Hydrogen Evolution. *Catalysts* **2023**, *13*, 1232. [CrossRef]
5. Sun, H.; Xu, X.; Kim, H.; Shao, Z.; Jung, W. Advanced electrocatalysts with unusual active sites for electrochemical water splitting. *InfoMat* **2023**, *6*, e12494. [CrossRef]
6. Pan, S.; Ma, Z.; Yang, W.; Dongyang, B.; Yang, H.; Lai, S.; Dong, F.; Yang, X.; Lin, Z. Magnesium incorporation activates perovskite cobaltites toward efficient and stable electrocatalytic oxygen evolution. *Mater. Rep. Energy* **2023**, *3*, 100212. [CrossRef]
7. Yang, Y.; Yang, Q.N.; Yang, Y.B.; Guo, P.F.; Feng, W.X.; Jia, Y.; Wang, K.; Wang, W.T.; He, Z.H.; Liu, Z.T. Enhancing Water Oxidation of Ru Single Atoms via Oxygen-Coordination Bonding with NiFe Layered Double Hydroxide. *ACS Catal.* **2023**, *13*, 2771–2779. [CrossRef]
8. Liu, S.X.; Zhang, H.W.; Hu, E.L.; Zhu, T.Y.; Zhou, C.Y.; Huang, Y.C.; Ling, M.; Gao, X.H.; Lin, Z. Boosting oxygen evolution activity of NiFe-LDH using oxygen vacancies and morphological engineering. *J. Mater. Chem. A* **2021**, *9*, 23697. [CrossRef]
9. Hu, J.; Liang, Y.Q.; Wu, S.L.; Li, Z.Y.; Shi, C.S.; Luo, S.Y.; Sun, H.J.; Zhu, S.L.; Cui, Z.D. Hierarchical nickel-iron layered double hydroxide composite electrocatalyst for efficient oxygen evolution reaction. *Mater. Today Nano* **2022**, *17*, 100150. [CrossRef]
10. Shen, K.; Tang, Y.; Zhou, Q.; Zhang, Y.; Ge, W.; Shai, X.; Deng, S.; Yang, P.; Deng, S.; Wang, J. Metal-organic framework-derived S-NiFe PBA coupled with NiFe layered double hydroxides as Mott-Schottky electrocatalysts for efficient alkaline oxygen evolution reaction. *Chem. Eng. J.* **2023**, *471*, 144827. [CrossRef]
11. Zhao, J.; Liao, N.; Luo, J. Transforming NiFe layered double hydroxide into NiFeP_x for efficient alkaline water splitting. *J. Mater. Chem. A* **2023**, *11*, 9682. [CrossRef]
12. Xu, H.; Xin, G.; Hu, W.; Zhang, Z.; Si, C.; Chen, J.; Lu, L.; Peng, Y.; Li, X. Single-atoms Ru/NiFe layered double hydroxide electrocatalyst: Efficient for oxidation of selective oxidation of 5-hydroxymethylfurfural and oxygen evolution reaction. *Appl. Catal. B Environ.* **2023**, *339*, 123157. [CrossRef]
13. Yin, X.; Hua, Y.N.; Gao, Z. In situ construction of S-doped NiFe-layered double hydroxide nanoarrays on porous reduced graphene oxide as efficient oxygen evolution electrocatalysts for electrolytic cells. *J. Energy Storage* **2023**, *73*, 109102. [CrossRef]
14. Liao, Y.Y.; He, R.C.; Pan, W.H.; Li, Y.; Wang, Y.Y.; Li, J.; Li, Y.X. Lattice distortion induced Ce-doped NiFe-LDH for efficient oxygen evolution. *Chem. Eng. J.* **2023**, *464*, 142669. [CrossRef]

15. Liu, S.L.; Wan, R.D.; Lin, Z.S.; Liu, Z.; Liu, Y.G.; Tian, Y.; Qin, D.D.; Tang, Z.H. Probing the Co role in promoting the OER and Zn-air battery performance of NiFe-LDH: A combined experimental and theoretical study. *J. Mater. Chem. A* **2022**, *10*, 5244. [[CrossRef](#)]
16. Wang, Y.Y.; Gao, Y.P.; Ma, L.X.; Xue, Y.Z.; Liu, Z.H.; Cui, H.L.; Zhang, N.; Jiang, R.B. Atomically Dispersed Fe-N₄ Sites and NiFe-LDH Sub-Nanoclusters as an Excellent Air Cathode for Rechargeable Zinc-Air Batteries. *ACS Appl. Mater. Interfaces* **2023**, *15*, 16732. [[CrossRef](#)]
17. Munonde, T.S.; Zheng, H.T. The impact of ultrasonic parameters on the exfoliation of NiFe LDH nanosheets as electrocatalysts for the oxygen evolution reaction in alkaline media. *Ultrason. Sonochem.* **2021**, *76*, 105664. [[CrossRef](#)] [[PubMed](#)]
18. Li, Y.; Guo, H.; Zhang, Y.; Zhang, H.; Zhao, J.; Song, R. Hollow Mo-doped NiS_x nanoarrays decorated with NiFe layered double-hydroxides for efficient and stable overall water splitting. *J. Mater. Chem. A* **2022**, *10*, 18989. [[CrossRef](#)]
19. Li, W.M.; Chen, S.H.; Zhong, M.X.; Wang, C.; Lu, X.F. Synergistic coupling of NiFe layered double hydroxides with Co-C nanofibers for high-efficiency oxygen evolution reaction. *Chem. Eng. J.* **2021**, *415*, 128879. [[CrossRef](#)]
20. Dresp, S.; Dionigi, F.; Klingenhof, M.; Merzdorf, T.; Schmies, H.; Drnec, J.; Poulain, A.; Strasser, P. Molecular Understanding of the Impact of Saline Contaminants and Alkaline pH on NiFe Layered Double Hydroxide Oxygen Evolution Catalysts. *ACS Catal.* **2021**, *11*, 6800. [[CrossRef](#)]
21. Rong, M.K.; Mo, Y.; Cao, Z.F.; Ma, X.; Wang, S.; Zhong, H. MoSe₂ regulates Ce-doped NiFe layered double hydroxide for efficient oxygen evolution reaction: The increase of active sites. *Int. J. Hydrogen Energy* **2022**, *47*, 18688. [[CrossRef](#)]
22. Xie, Q.X.; Ren, D.; Bai, L.C.; Ge, R.L.; Zhou, W.H.; Bai, L.; Xie, W.; Wang, J.H.; Graetzel, M.; Luo, J.S. Investigation of nickel iron layered double hydroxide for water oxidation in different pH electrolytes. *Chin. J. Catal.* **2023**, *44*, 127. [[CrossRef](#)]
23. Shi, K.; Sun, Z.; Yuan, M.; Zhao, Y.; Sun, G. "Polyoxometalate electron sponge" induces the accurate regulation of electron states at Ni sites to enhance oxidation of water. *J. Colloid Interface Sci.* **2023**, *657*, 37. [[CrossRef](#)] [[PubMed](#)]
24. Arshad, F.; Munir, A.; Tahir, A.; Hussain, S.Z.; Jilani, A.; Hussain, A.; Ullah, N.; Sher, F.; Hussain, I. Microwave-assisted growth of spherical core-shell NiFe LDH@Cu₂O nanostructures for electrocatalytic water oxidation reaction. *Int. J. Hydrogen Energy* **2023**, *48*, 4719. [[CrossRef](#)]
25. Wen, Q.L.; Wang, S.Z.; Wang, R.W.; Huang, D.J.; Fang, J.K.; Liu, Y.W.; Zhai, T.Y. Nanopore-rich NiFe LDH targets the formation of the high-valent nickel for enhanced oxygen evolution reaction. *Nano Res.* **2023**, *16*, 2286. [[CrossRef](#)]
26. Liu, X.; Wang, X.; Yuan, X.; Dong, W.; Huang, F. Rational composition and structural design of in situ grown nickel-based electrocatalysts for efficient water electrolysis. *J. Mater. Chem. A* **2016**, *4*, 167. [[CrossRef](#)]
27. Chen, Z.W.; Ju, M.; Sun, M.Z.; Jin, L.; Cai, R.M.; Wang, Z.; Dong, L.; Peng, L.M.; Long, X.; Huang, B.L.; et al. TM LDH Meets Birnessite: A 2D-2D Hybrid Catalyst with Long-Term Stability for Water Oxidation at Industrial Operating Conditions. *Angew. Chem. -Int. Ed.* **2021**, *60*, 9699. [[CrossRef](#)]
28. Huang, J.W.; Li, K.; Wang, L.; She, H.D.; Wang, Q.Z. In situ conversion builds MIL-101@NiFe-LDH heterojunction structures to enhance the oxygen evolution reaction. *Chin. Chem. Lett.* **2022**, *33*, 3787. [[CrossRef](#)]
29. Dong, Y.; Komarneni, S.; Wang, N.; Hu, W.C.; Huang, W.Y. An in situ anion exchange induced high-performance oxygen evolution reaction catalyst for the pH-near-neutral potassium borate electrolyte. *J. Mater. Chem. A* **2019**, *7*, 6995. [[CrossRef](#)]
30. Mohammed-Ibrahim, J. A review on NiFe-based electrocatalysts for efficient alkaline oxygen evolution reaction. *J. Power Sources* **2020**, *448*, 227375. [[CrossRef](#)]
31. Li, S.Z.; Liu, J.Y.; Duan, S.; Wang, T.Y.; Li, Q. Tuning the oxygen evolution electrocatalysis on NiFe-layered double hydroxides via sulfur doping. *Chin. J. Catal.* **2020**, *41*, 847. [[CrossRef](#)]
32. Zhu, Y.; Wang, X.; Zhu, X.H.; Wu, Z.X.; Zhao, D.S.; Wang, F.; Sun, D.M.; Tang, Y.W.; Li, H.; Fu, G.T. Improving the Oxygen Evolution Activity of Layered Double-Hydroxide via Erbium-Induced Electronic Engineering. *Small* **2023**, *19*, e2206531. [[CrossRef](#)] [[PubMed](#)]
33. Xu, H.; Guo, T.; Lei, X.; Guo, S.; Liu, Q.; Lu, J.; Zhang, T. Enhancing Electrocatalytic Water Oxidation of NiFe-LDH Nanosheets via Bismuth-Induced Electronic Structure Engineering. *ACS Appl. Mater. Interfaces* **2023**, *15*, 58784. [[CrossRef](#)] [[PubMed](#)]
34. Zheng, Y.Q.; Deng, H.Y.; Feng, H.R.; Luo, G.Q.; Tu, R.; Zhang, L.M. Triethanolamine-assisted synthesis of NiFe layered double hydroxide ultrathin nanosheets for efficient oxygen evolution reaction. *J. Colloid Interface Sci.* **2023**, *629*, 610. [[CrossRef](#)] [[PubMed](#)]
35. Liu, J.; Wang, J.S.; Zhang, B.; Ruan, Y.J.; Lv, L.; Ji, X.; Xu, K.; Miao, L.; Jiang, J.J. Hierarchical NiCo₂S₄@NiFe LDH Heterostructures Supported on Nickel Foam for Enhanced Overall-Water-Splitting Activity. *ACS Appl. Mater. Interfaces* **2017**, *9*, 15364. [[CrossRef](#)] [[PubMed](#)]
36. Li, M.; Li, H.; Jiang, X.C.; Jiang, M.Q.; Zhan, X.; Fu, G.T.; Lee, J.M.; Tang, Y.W. Gd-induced electronic structure engineering of a NiFe-layered double hydroxide for efficient oxygen evolution. *J. Mater. Chem. A* **2021**, *9*, 2999. [[CrossRef](#)]
37. Shen, J.; Zhang, P.; Xie, R.S.; Chen, L.; Li, M.T.; Li, J.P.; Ji, B.Q.; Hu, Z.Y.; Li, J.J.; Song, L.X.; et al. Controlled Self-Assembled NiFe Layered Double Hydroxides/Reduced Graphene Oxide Nanohybrids Based on the Solid-Phase Exfoliation Strategy as an Excellent Electrocatalyst for the Oxygen Evolution Reaction. *ACS Appl. Mater. Interfaces* **2019**, *11*, 13545. [[CrossRef](#)] [[PubMed](#)]
38. Zhang, Z.; Zhao, X.; Luo, H.; Feng, X.; Chen, H. Design of wood-based self-supporting metal catalyst based on NiCo₂O₄ bridge for efficient oxygen evolution. *Chem. Eng. J.* **2023**, *477*, 147289. [[CrossRef](#)]
39. Shen, B.; Feng, Y.; Wang, Y.; Sun, P.; Yang, L.; Jiang, Q.; He, H.; Huang, H. Holey MXene nanosheets intimately coupled with ultrathin Ni-Fe layered double hydroxides for boosted hydrogen and oxygen evolution reactions. *Carbon* **2023**, *212*, 118141. [[CrossRef](#)]

40. Feng, X.; Jiao, Q.; Chen, W.; Dang, Y.; Dai, Z.; Suib, S.L.; Zhang, J.; Zhao, Y.; Li, H.; Feng, C. Cactus-like NiCo₂S₄@NiFe LDH hollow spheres as an effective oxygen bifunctional electrocatalyst in alkaline solution. *Appl. Catal. B Environ.* **2021**, *286*, 119869. [[CrossRef](#)]
41. Lu, Z.Y.; Xu, W.W.; Zhu, W.; Yang, Q.; Lei, X.D.; Liu, J.F.; Li, Y.P.; Sun, X.M.; Duan, X. Three-dimensional NiFe layered double hydroxide film for high-efficiency oxygen evolution reaction. *Chem. Commun.* **2014**, *50*, 6479. [[CrossRef](#)] [[PubMed](#)]
42. Xu, X.; Pan, Y.; Ge, L.; Chen, Y.; Mao, X.; Guan, D.; Li, M.; Zhong, Y.; Hu, Z.; Peterson, V.K.; et al. High-Performance Perovskite Composite Electrocatalysts Enabled by Controllable Interface Engineering. *Small* **2021**, *17*, 2101573. [[CrossRef](#)]
43. Du, Y.; Liu, D.; Li, T.; Yan, Y.; Liang, Y.; Yan, S.; Zou, Z. A phase transformation-free redox couple mediated electrocatalytic oxygen evolution reaction. *Appl. Catal. B Environ.* **2022**, *306*, 121146. [[CrossRef](#)]
44. Cao, S.; Huang, H.; Shi, K.; Wei, L.; You, N.; Fan, X.; Yang, Z.; Zhang, W. Engineering superhydrophilic/superaerophobic hierarchical structures of Co-CH@NiFe-LDH/NF to boost the oxygen evolution reaction. *Chem. Eng. J.* **2021**, *422*, 130123. [[CrossRef](#)]
45. Yang, R.; Zhou, Y.; Xing, Y.; Li, D.; Jiang, D.; Chen, M.; Shi, W.; Yuan, S. Synergistic coupling of CoFe-LDH arrays with NiFe-LDH nanosheet for highly efficient overall water splitting in alkaline media. *Appl. Catal. B Environ.* **2019**, *253*, 131. [[CrossRef](#)]
46. Yang, Y.; Xie, Y.; Yu, Z.; Guo, S.; Yuan, M.; Yao, H.; Liang, Z.; Lu, Y.R.; Chan, T.S.; Li, C.; et al. Self-supported NiFe-LDH@CoS_x nanosheet arrays grown on nickel foam as efficient bifunctional electrocatalysts for overall water splitting. *Chem. Eng. J.* **2021**, *419*, 129512. [[CrossRef](#)]
47. Hu, L. Modulating interfacial electronic structure of CoNi LDH nanosheets with Ti₃C₂T MXene for enhancing water oxidation catalysis. *Chem. Eng. J.* **2020**, *398*, 125605. [[CrossRef](#)]
48. Wen, Y. Synergistic cerium doping and MXene coupling in layered double hydroxides as efficient electrocatalysts for oxygen evolution. *J. Energy Chem.* **2021**, *52*, 412–420. [[CrossRef](#)]
49. Yu, M. Boosting electrocatalytic oxygen evolution by synergistically coupling layered double hydroxide with MXene. *Nano Energy* **2018**, *44*, 181–190. [[CrossRef](#)]
50. Zhang, C. Layer-by-layer assembly of exfoliated layered double hydroxide nanosheets for enhanced electrochemical oxidation of water. *J. Mater. Chem. A* **2016**, *4*, 11516–11523. [[CrossRef](#)]
51. Zhao, L. Facile synthesis and efficient electrochemical water splitting of bifunctional nanostructured Ni-based layered double hydroxide/sulfide composite. *J. Alloys Compd.* **2022**, *910*, 164880. [[CrossRef](#)]

Disclaimer/Publisher's Note: The statements, opinions and data contained in all publications are solely those of the individual author(s) and contributor(s) and not of MDPI and/or the editor(s). MDPI and/or the editor(s) disclaim responsibility for any injury to people or property resulting from any ideas, methods, instructions or products referred to in the content.